


ORIGINAL ARTICLE

Open Access



MRI-based machine-learning radiomics of the liver to predict liver-related events in hepatitis B virus-associated fibrosis

Yuankai Luo^{1,2}, Qinian Luo³, Yaobo Wu⁴, Shaorui Zhang⁵, Huan Ren⁶, Xiaofeng Wang⁴, Xiujuan Liu⁷, Qin Yang⁴, Weiguo Xu², Qingsong Wu^{1*} and Yong Li^{2*} 

Abstract

Background The onset of liver-related events (LREs) in fibrosis indicates a poor prognosis and worsens patients' quality of life, making the prediction and early detection of LREs crucial. The aim of this study was to develop a radiomics model using liver magnetic resonance imaging (MRI) to predict LRE risk in patients undergoing antiviral treatment for chronic fibrosis caused by hepatitis B virus (HBV).

Methods Patients with HBV-associated liver fibrosis and liver stiffness measurements ≥ 10 kPa were included. Feature selection and dimensionality reduction techniques identified discriminative features from three MRI sequences. Radiomics models were built using eight machine learning techniques and evaluated for performance. Shapley additive explanation and permutation importance techniques were applied to interpret the model output.

Results A total of 222 patients aged 49 ± 10 years (mean \pm standard deviation), 175 males, were evaluated, with 41 experiencing LREs. The radiomics model, incorporating 58 selected features, outperformed traditional clinical tools in prediction accuracy. Developed using a support vector machine classifier, the model achieved optimal areas under the receiver operating characteristic curves of 0.94 and 0.93 in the training and test sets, respectively, demonstrating good calibration.

Conclusion Machine learning techniques effectively predicted LREs in patients with fibrosis and HBV, offering comparable accuracy across algorithms and supporting personalized care decisions for HBV-related liver disease.

Relevance statement Radiomics models based on liver multisequence MRI can improve risk prediction and management of patients with HBV-associated chronic fibrosis. In addition, it offers valuable prognostic insights and aids in making informed clinical decisions.

Key Points

- Liver-related events (LREs) are associated with poor prognosis in chronic fibrosis.
- Radiomics models could predict LREs in patients with hepatitis B-associated chronic fibrosis.
- Radiomics contributes to personalized care choices for patients with hepatitis B-associated fibrosis.

Keywords Hepatitis B (chronic), Liver fibrosis, Machine learning, Magnetic resonance imaging, Radiomics

Yuankai Luo, Qinian Luo, Yaobo Wu and Shaorui Zhang contributed equally to this work.

*Correspondence:

Qingsong Wu
13826368658@163.com

Yong Li
929125300@qq.com

Full list of author information is available at the end of the article



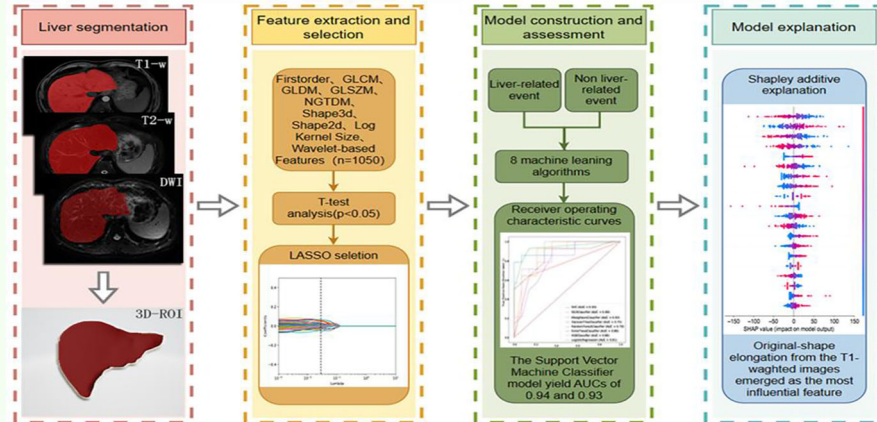
© The Author(s) 2025. **Open Access** This article is licensed under a Creative Commons Attribution 4.0 International License, which permits use, sharing, adaptation, distribution and reproduction in any medium or format, as long as you give appropriate credit to the original author(s) and the source, provide a link to the Creative Commons licence, and indicate if changes were made. The images or other third party material in this article are included in the article's Creative Commons licence, unless indicated otherwise in a credit line to the material. If material is not included in the article's Creative Commons licence and your intended use is not permitted by statutory regulation or exceeds the permitted use, you will need to obtain permission directly from the copyright holder. To view a copy of this licence, visit <http://creativecommons.org/licenses/by/4.0/>.

Graphical Abstract

MRI-based machine-learning radiomics of the liver to predict liver-related events in hepatitis B virus-associated fibrosis

- Liver-related events (LREs) are associated with a poor prognosis in chronic fibrosis.
- Radiomics contributes to personalized care choices for individuals with hepatitis B-associated fibrosis.

MRI-based radiomics may predict hepatitis B associated to chronic cirrhosis.



**Eur Radiol Exp (2025) Luo YK, Luo QN, Wu YB et al;
DOI: 10.1186/s41747-025-00602-0**

Background

Hepatitis B virus (HBV) infection is a major global health concern [1]. About 20% of those infected develop chronic hepatitis, and 10–20% of these cases progress to cirrhosis, a progressive liver disease marked by fibrosis and impaired liver function [2]. Although oral antiviral therapy is the standard treatment for HBV-associated fibrosis [3, 4], liver-related events (LREs), such as ascites, variceal bleeding, hepatorenal syndrome, hepatic encephalopathy, and hepatocellular carcinoma, may still occur [5–8]. LREs in fibrosis indicate a poor prognosis and diminish health-related quality of life [9]. Early identification and prediction are essential for implementing interventions that improve patient outcomes.

Magnetic resonance imaging (MRI), a powerful tool for diagnosing and managing liver disease, enables accurate, noninvasive detection and characterization. Its excellent soft tissue resolution provides detailed insights into liver lesions and fibrosis staging [10, 11]. Recent advances in machine learning have enabled the analysis of quantitative imaging features, known as radiomics [12]. These features capture subtle tissue variations on MRI and hold promise for predicting treatment response and prognosis across various diseases [13, 14].

Research on liver MRI-based radiomics for predicting LREs in HBV-associated fibrosis remains limited. Most

studies rely on clinical factors or serum biomarkers [15, 16], underutilizing imaging data. While radiological imaging is the only noninvasive method for capturing liver disease's spatial heterogeneity, its full potential has yet to be realized [17]. Therefore, we employed various machine learning algorithms to develop predictive models using MRI radiomics features to identify imaging factors most associated with HBV-associated fibrosis and assess LRE risk.

Methods

Patient selection

This study adhered to the Declaration of Helsinki and was approved by the Ethics Committee of Zhuhai People's Hospital (Approval Number 37 (2021)). Due to its retrospective design, informed consent was waived. All patient records and information were anonymized and de-identified prior to analysis.

This study retrospectively analyzed the data of patients with HBV who received antiviral treatment between January 2022 and July 2023. We included all consecutive patients who met the inclusion and exclusion criteria. Patient data were retrieved from the hospital's electronic medical records. The inclusion criteria were: (1) age 18–75 years; (2) clinical diagnosis of chronic hepatitis B with hepatitis B surface antigen positivity for at least six months

and HBV deoxyribonucleic acid–DNA levels $> 5 \log_{10}$ copies/mL; (3) liver stiffness measurement (LSM) ≥ 10 kPa; and (4) current oral antiviral therapy for chronic hepatitis B. The exclusion criteria were: (1) no upper abdominal MRI before the LRE; (2) inadequate MRI quality due to artifacts, low signal-to-noise ratios, poor resolution, and other related issues; (3) Absence of laboratory tests essential for the assessment of liver function and complete blood, such as LSM, alanine aminotransferase (ALT), aspartate aminotransferase (AST), and platelet count; (4) poor medication adherence; and (5) loss to follow-up.

Follow-up and LREs

All patients received antiviral therapy per standard guidelines [3], including entecavir, tenofovir, adefovir dipivoxil, and tenofovir dipivoxil. Follow-up began after the MRI, and only LREs occurring post-MRI were considered. All patients underwent MRI using a 3.0-T unit (Ingenia CX, Philips; Discovery 750 W, GE Healthcare) or a 1.5-T unit (SIGNA™ Creator, GE Healthcare). The index diagnostic test was an upper abdominal MRI with no reference standard diagnostic test. The primary endpoint was LRE development. Medical records of all enrolled patients were reviewed until July 2023 to identify LREs, including hepatorenal syndrome, ascites, hepatic encephalopathy, upper gastrointestinal variceal bleeding, and hepatocellular carcinoma. The last one was confirmed using at least two of the following radiological techniques: contrast-enhanced ultrasound, contrast-enhanced computed tomography, multi-sequence MRI, or gadolinium ethoxybenzyl diethylenetriaminepentaacetic acid-enhanced MRI [18].

Clinical data collection

Baseline demographic data (age, sex, weight, height, hypertension history, and alcoholism) and laboratory parameters (platelet count, aminotransferases, alpha-fetoprotein, albumin, and total bilirubin) were collected. LSMs conducted within six months before or after MRI were also included. We performed LSMs using transient elastography (Fibro Touch-C, Haisikaier). All procedures were performed by a skilled operator following a standard protocol. Patients fasted beforehand, and at least 10 valid measurements were obtained per patient. The operator recorded the average number of valid measurements, and only assessments meeting validity criteria were included in the analysis.

Image acquisition

All patients underwent an upper abdominal MRI. To extract imaging features, their images were retrieved from the picture archiving and communication system.

Two radiologists—Reader 1 (Y.K.L.) and Reader 2 (X.J.L.)—with 7 and 15 years of experience, respectively,

assessed MRI image quality to determine eligibility for image segmentation and radiomics feature extraction. Both readers manually delineated the liver area on each cross-sectional MRI slice using ITK-SNAP software version 3.8 (www.itksnap.org). We carefully outlined the liver in each layer without exceeding its margin to minimize the potential impact on neighboring organs. Initially, images from 30 randomly selected patients were segmented by both readers. For cases with subjective errors, such as unclear liver edges due to respiratory artifacts, consensus was reached through discussion to ensure segmentation consistency. A week later, reader one repeated the procedure on the same 30 patients and segmented the remaining 192.

Feature extraction and normalization

PyRadiomics, an open-source Python package (<https://www.python.org/>), was used to extract radiomics features from regions of interest. Extracted features included first-order features, Neighborhood Gray-Tone Difference Matrix, Gray Level Co-Occurrence Matrix, Gray Level Dependence Matrix, Gray Level Size Zone Matrix (GLSZM), Shape3D, Shape2D, Laplacian of Gaussian filter (kernel size: 4×5 pixels, height \times width), and Wavelet-Based Features [19], totaling 1,050 features. We performed data cleaning and used a *t*-test to identify statistically significant features from the images ($p < 0.05$). Feature data were standardized using the *z*-score method to eliminate the influence of varying units and dimensions.

Feature selection and radiomics model development

We first conducted intra-group assessments to evaluate the consistency of the same reader's segmentations for the same patient at different time points, selecting features with strong reproducibility. Next, inter-group assessments measured segmentation consistency between readers for the same patient. Features were included in the analysis only if their intraclass correlation coefficients exceeded 0.75 in both assessments. Using computer-generated randomization, patients were assigned to training and test cohorts in a 7:3 ratio. To prevent overfitting, we used the least absolute shrinkage and selection operator (LASSO) algorithm to build a regression model, leveraging its strong dimensionality reduction capability to identify the top predictive features with nonzero LASSO coefficients. Eight machine learning algorithms, including logistic regression, support vector machine, random forest, extreme gradient boosting—XGBoost classifier, K-Nearest Neighbors, decision tree, extra trees, and stochastic gradient descent classifiers, were employed for feature selection and radiomics model development. The machine learning library Scikit-learn version 1.2.0 (<https://scikit-learn.org/stable/>) in Python (V3.7.0) was

used to model and predict LREs based on quantitative radiomics features. The models' inputs comprised features selected by LASSO, while the outputs represented follow-up results for each case. Using the specified characteristics, a 10-fold cross-validation of the training set validated the radiomics models' effectiveness. The training process used a grid-search method to optimize hyperparameters for each model. Some representative hyperparameter combinations from the grid search are shown in Supplemental File 1 (Feature extraction). The area under the receiver operating characteristic curve (AUC) was analyzed to determine the most effective model.

Validation and comparison of radiomics models

Model discrimination was assessed using a calibration plot. Calibration curves illustrate the alignment between model predictions and actual outcomes, offering an intuitive measure of reliability essential for gaining researchers' and clinicians' trust. Receiver operating characteristic curve analyses were also performed on the fibrosis-4 index, aspartate aminotransferase to platelet ratio index, and LSM, comparing these traditional clinical methods with our radiomics models. This comparison helps establish the role of MRI-based machine learning radiomics in predicting LREs.

Machine learning explainable tool

The models were interpreted using SHapley Additive exPlanation–SHAP, which accurately quantifies each feature's contribution to the final predictions [20]. These values allowed us to assess how each predictor positively or negatively influenced the target variable. Each radiomics feature was analyzed using its corresponding values. Additionally, the importance of permutation was applied to assess each feature's significance in predicting outcomes. This method estimates the importance of observed

feature distribution by iteratively permuting the result vector within a noninformative context [21].

Statistical analyses

Descriptive statistics (means and standard deviations) were used for continuous variables with a normal distribution. Conversely, descriptive measures (median/interquartile range and minimum/maximum values) were used for continuous variables without a normal distribution. The AUC was calculated to assess model performance. All statistical tests were conducted as two-sided tests, with a significance threshold set at $p < 0.05$. All statistical analyses were performed using the R statistical package V4.1.2 (<https://www.r-project.org/>).

Results

Patient characteristics

This study enrolled 222 patients aged 18 to 75 years with HBV-related fibrosis (LSM ≥ 10 kPa) who underwent antiviral treatment. LRE rates did not differ significantly between the training and test sets (Table 1). Similarly, no significant differences were observed in clinical indicators, including sex, age, platelet count, and LSMs, between the two groups. Fibrosis-4 scores and aspartate aminotransferase to platelet ratio index also showed no significant differences between the training and test cohorts (Table 2). Figure 1 shows the baseline characteristics of the included patients. The training and test sets comprised 155 and 67 patients, respectively, with 28 and 13 patients developing LREs (41 in total) (Fig. 2).

Feature selection and model construction

After the independent sample t -test and z -score standardization, 1,050 features were included in the LASSO regression. Figure 3 illustrates the feature selection process for predicting LREs. Ultimately, 58 features were selected for further analysis. Among them, Wavelet-LHH

Table 1 Scanning parameters for magnetic resonance images

MRI scanner	Number	Sequence	TR/TE (ms)	Slice thickness (mm)	Slice gap (mm)	Field of view (mm)	Scanning matrix
3.0-T Ingenia CX, Philips	79	T1-w	3.22/0	4	2	448 × 448	268 × 265
		T2-w	2,725/86	6	7	432 × 432	296 × 258
		DWI	1,617/15	6	7	288 × 288	140 × 137
3.0-T Discovery 750 W, GE Healthcare	59	T1-w	4.54/1.67	5	2.5	512 × 512	256 × 200
		T2-w	6,000/79	6	7	512 × 512	320 × 320
		DWI	6,000/28	6	7	256 × 256	128 × 128
1.5-T SIGNA™ Creator, GE Healthcare	84	T1-w	6.16/3.13	5	2.5	256 × 256	256 × 192
		T2-w	3,157/82	6	7	512 × 512	320 × 320
		DWI	2,500/27	6	7	256 × 256	128 × 128

MRI Magnetic resonance imaging, TR Repetition time, TE Echo time, DWI Diffusion-weighted imaging, T1-w T1-weighted imaging, T2-w T2-weighted imaging

Table 2 Baseline characteristics of the 222 patients with a liver stiffness measurement (LSM) ≥ 10 kPa

Characteristic	Cohort			p-value ^b
	Overall n = 222 ^a	Training n = 155 ^a	Test n = 67 ^a	
Age (years)	49 ± 11	49 ± 11	49 ± 10	0.933
Sex (n, %)				0.271
Female	46 (20.81)	29 (18.83)	17 (25.37)	
Male	175 (79.19)	125 (81.17)	50 (74.63)	
Alcoholism (n, %)				0.164
No	179 (81.00)	121 (78.57)	58 (86.57)	
Yes	42 (19.00)	33 (21.43)	9 (13.43)	
Hyperlipidemic (n, %)				0.284
No	197 (89.14)	135 (87.66)	62 (92.54)	
Yes	24 (10.86)	19 (12.34)	5 (7.46)	
Diabetes (n, %)				0.943
No	128 (80.50)	90 (80.36)	38 (80.85)	
Yes	31 (19.50)	22 (19.64)	9 (19.15)	
BMI (kg/m ²)	24.0 ± 3.8	24.3 ± 4.1	23.3 ± 2.9	0.045
LSM (kPa)	13.70 ± 3.92	13.63 ± 4.14	13.80 ± 3.42	0.746
AFP (ng/mL)	7 ± 20	8 ± 24	5 ± 6	0.114
PIVKA-2 (mAu/mL)	25 ± 12	25 ± 13	25 ± 9	0.790
PLT (U/L)	178 ± 64	178 ± 65	178 ± 63	0.953
AST (U/L)	34 ± 27	35 ± 31	31 ± 15	0.187
ALT (U/L)	42 ± 70	45 ± 82	35 ± 23	0.183
ALP (U/L)	94 ± 33	95 ± 37	92 ± 24	0.570
Tbil (μmol/L)	17 ± 10	17 ± 11	15 ± 9	0.229
GGT (U/L)	45 ± 44	47 ± 49	39 ± 26	0.112
ALB (U/L)	44.1 ± 3.9	44.0 ± 4.2	44.2 ± 3.3	0.635
URIC (μmol/L)	358 ± 89	358 ± 92	359 ± 83	0.905
GLU (mmol/L)	5.66 ± 0.97	5.65 ± 1.03	5.68 ± 0.81	0.886
APRI	0.56 ± 0.48	0.59 ± 0.55	0.48 ± 0.27	0.083
FIB-4	1.85 ± 1.37	1.90 ± 1.47	1.74 ± 1.11	0.404

AFP Alpha-fetoprotein, ALB Albumin, ALP Alkaline phosphatase, ALT Alanine transaminase, APRI Aminotransferase-to-platelet ratio index, AST Aspartate aminotransferase, BMI Body mass index, FIB-4 Fibrosis 4 score, GGT Glutamyl transpeptidase, GLU Fasting blood glucose, LSM Liver stiffness measurement, PIVKA-2 Prothrombin induced by vitamin K absence or antagonist II, PLT Platelet, Tbil Total bilirubin, URIC Serum uric acid

^a Mean ± standard deviation or n (%)

^b Welch two-sample t-test; Pearson's χ^2 test

Gray-Level Run Length Matrix (GLRLM) Gray-Level Non-Uniformity Normalized from diffusion-weighted imaging (DWI) had the highest absolute regression coefficient, making it the most influential feature in enhancing predictive performance.

Using the top 58 features identified in the selection process, eight radiomics models were developed with corresponding classifiers to predict LREs in the training and test sets (Fig. 4a, b). The support vector machine classifier radiomics model exhibited superior predictive performance, achieving AUCs of 0.94 and 0.93 in the

training and test sets, respectively, outperforming all other classifiers. The model details and the corresponding coefficient weight map of the features are shown in Supplemental File 2 (Table S1 and Fig. S1). Patients with LREs had significantly higher radiomics scores than those without LREs across the training, test, and overall cohorts (Supplemental Fig. S2).

Clinical application and apparent performance of the model

The calibration curves of the eight radiomics models illustrate the agreement between predictions and observations, showing some deviation from a perfect fit (Fig. 5). The AUCs of traditional clinical tools are presented in Supplemental Fig. S3. The overall AUC of the radiomics models exceeded that of traditional clinical tools, highlighting their clinical utility and effectiveness. Relative confusion matrices and detailed model performance metrics, including accuracy, specificity, recall, precision, and F1 score, are provided in Supplemental Fig. S4.

Explanation of model prediction

Permutation importance results were ranked in descending order based on feature importance scores (Supplemental Fig. S5) to identify the most influential features in model predictions, aiding in understanding how the model identifies key predictors. The average log-sigma-3-0-mm-3D GLSZM Gray-Level Non-Uniformity Normalized in the DWI exhibited the highest predictive value across all prediction horizons. Additionally, SHapley Additive exPlanation values were used to determine the positive and negative relationships between the radiomics signature and LRE outcomes. In Fig. 6, the horizontal position indicates whether a specific value contributes to a higher or lower prediction. At the same time, the color represents whether the variable is high (red) or low (blue) for that observation.

Discussion

Oral antiviral therapy is increasingly recognized as a standard treatment for delaying HBV-related fibrosis and cirrhosis. However, some patients still develop LREs, such as hepatocellular carcinoma or hepatic decompensation. Previous predictive studies on HBV-related fibrosis have primarily focused on clinical features, while the potential of radiological imaging as a noninvasive method to capture the spatial heterogeneity of liver disease remains underexplored. Remarkably, efforts to identify fibrosis features that predict responses to antiviral treatments have largely overlooked this issue [22, 23]. The heterogeneity of the liver microenvironment may contribute to variability in treatment response. Therefore, we aimed to predict LRE risk in liver fibrosis using machine learning

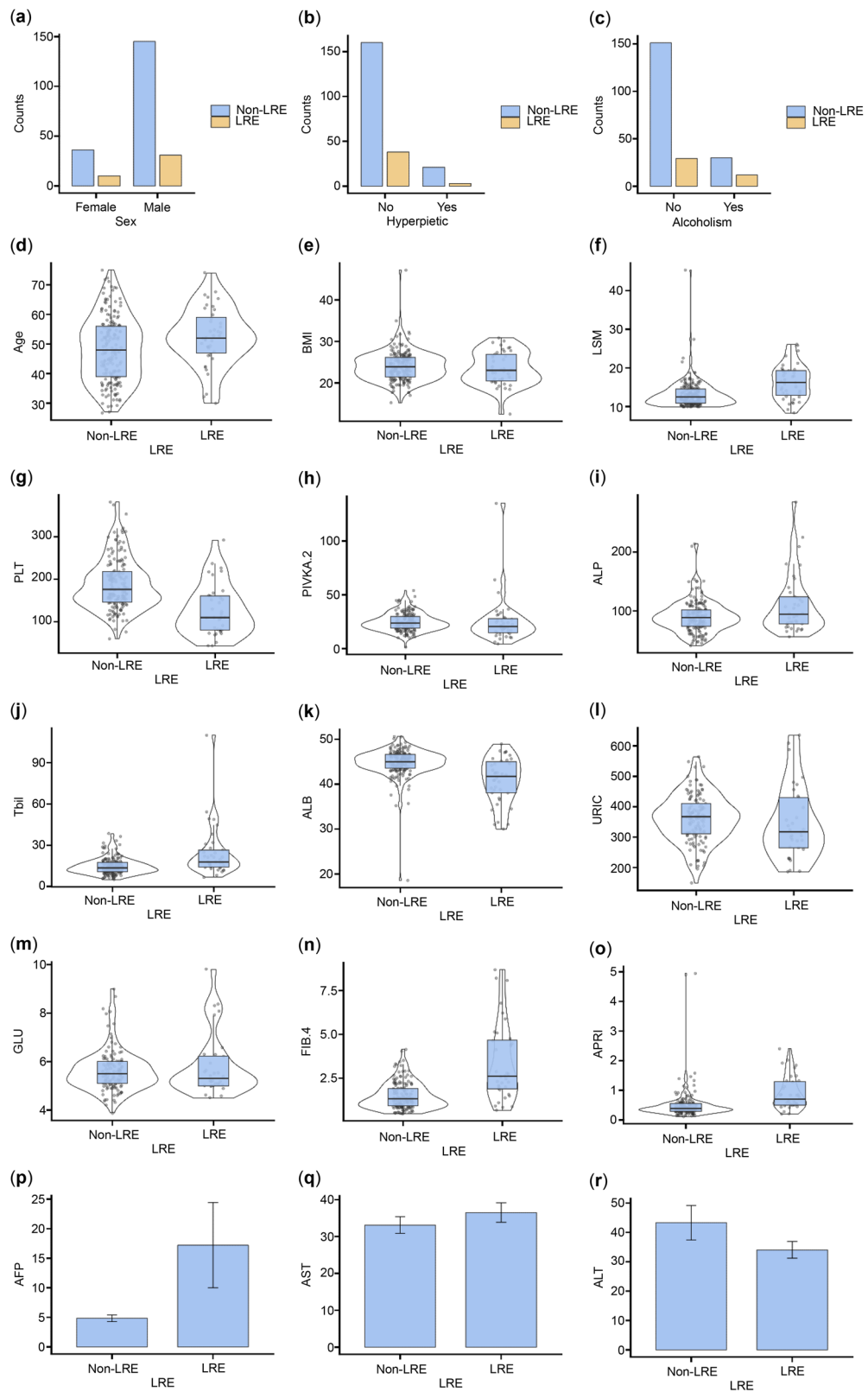


Fig. 1 (See legend on next page.)

(see figure on previous page)

Fig. 1 Baseline characteristics of the included patients. The figure compares demographic and clinical characteristics between the LRE and non-LRE groups. Data presentation: bar charts for categorical variables shown as counts (a–c); violin/box plots for continuous variables shown as median with interquartile range (IQR) (d–o); bar charts with error bars for continuous variables shown as mean with standard deviation (SD) (p–r). AFP, Alpha-fetoprotein; ALB, Albumin; ALP, Alkaline phosphatase; ALT, Alanine transaminase; APRI, Aminotransferase-to-platelet ratio index; AST, Aspartate aminotransferase; BMI, Body mass index; FIB-4, Fibrosis 4 score; GGT, Glutamyl transpeptidase; GLU, Fasting blood glucose; LRE, Liver-related event; LSM, Liver stiffness measurement; Non-LRE, Patients without liver-related event; PIVKA-2, Prothrombin induced by vitamin K absence or antagonist II; PLT, Platelet; Tbil, Total bilirubin; URIC, Serum uric acid

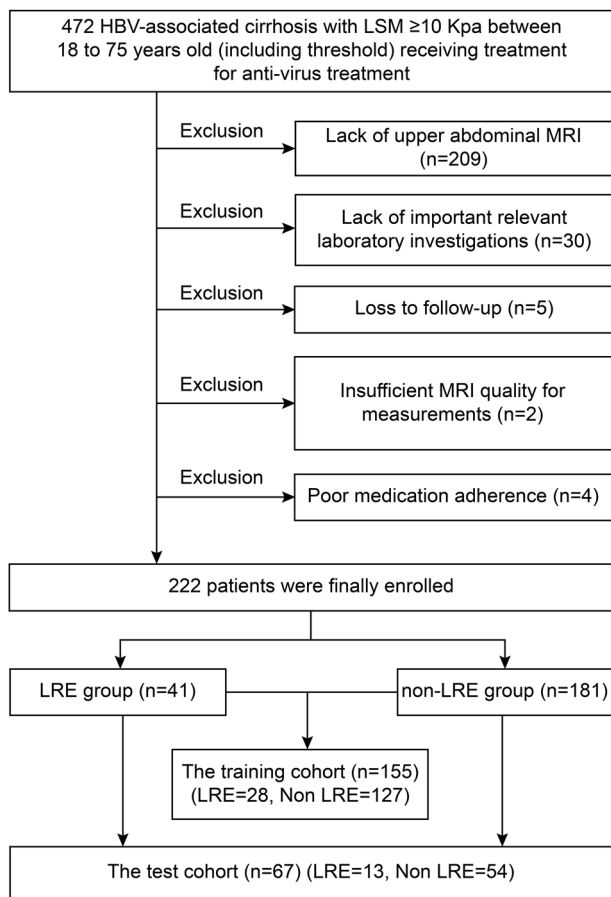


Fig. 2 Flowchart showing the inclusion and exclusion of patients in this study. HBV, Hepatitis B virus; LRE, Liver-related event; LSM, Liver stiffness measurement; MRI, Magnetic resonance imaging

radiomics methods based on multi-sequence MRI of the whole liver.

To our knowledge, this is the first study to predict LREs in patients with chronic HBV-associated fibrosis using an MRI-based radiomics approach. This method offered a more comprehensive assessment than computed tomography- or ultrasound-based radiomics [24, 25] and significantly improved prediction accuracy with multi-sequence MRI. We assessed the impact of computational dimensionality—two-dimensional (2D) slice-wise *versus* three-dimensional (3D) volumetric feature extraction—using identical 3D volume of interest masks for

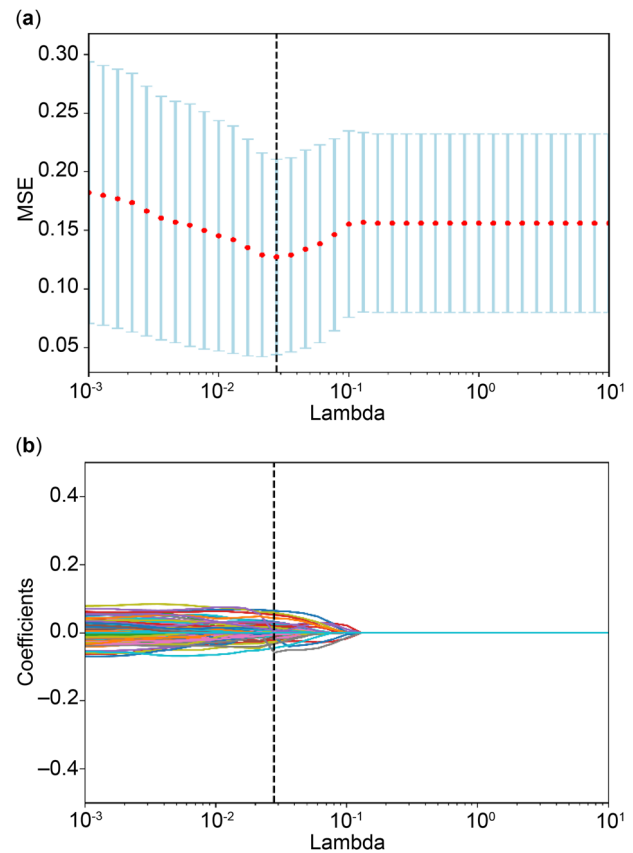


Fig. 3 The least absolute shrinkage and selection operator (LASSO) algorithms. **a** LASSO regression feature screening chart, with dashed lines indicating the selected optimal λ value of 0.02782559402207126, along with the location of one standard error, which generates the lowest possible mean squared error (MSE). **b** The LASSO convergence coefficient graph of the different omics features in the training group representing the curve of variation in image omics feature coefficients with $\log(\lambda)$

both approaches. This design isolates computational methodology effects from volume of interest spatial variations, enabling a direct comparison of texture characterization capabilities.

MRI-based quantitative radiomics exhibited strong performance as a noninvasive, high-throughput approach for predicting LREs in patients with HBV-related fibrosis. The support vector machine classifier achieved AUCs of 0.94 and 0.93 in the training and test sets, respectively. Support vector machine has been recognized as highly effective for

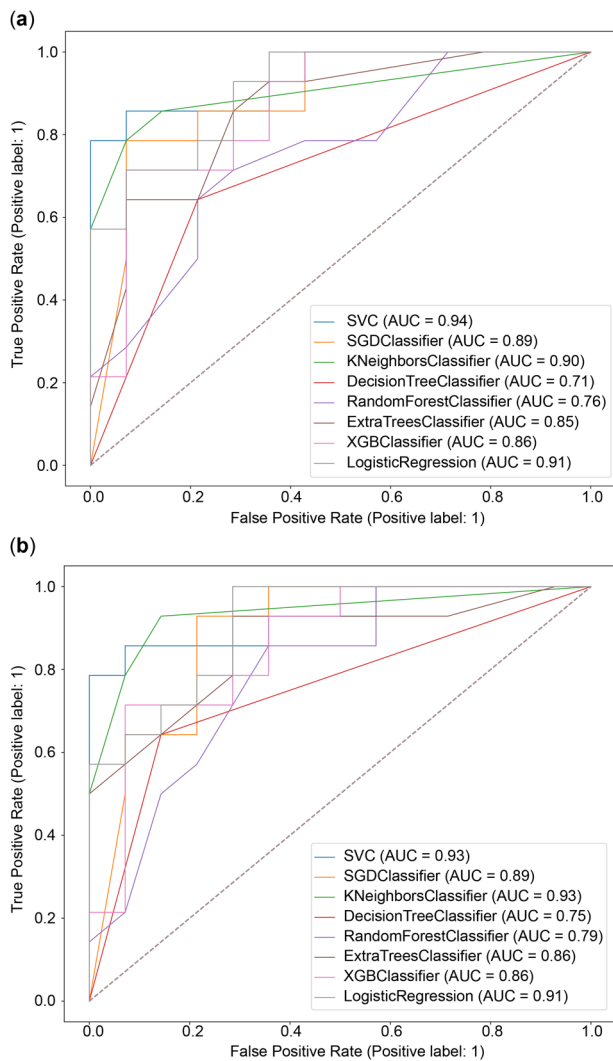


Fig. 4 Receiver operating characteristic (ROC) curves and the corresponding calibrations. **a** ROC curves of the radiomics models from different methods for the training cohort. **b** ROC curves of the radiomics models from different methods for the test cohort. SGD, Stochastic gradient descent; SVC, Support vector machine classifier; AUC, Area under the curve; XGB, Extreme gradient boosting

radiomics analysis and is well-suited for this classification task [26, 27]. The AUCs of the remaining seven machine learning algorithms were all ≥ 0.71 in both cohorts, with most exceeding 0.85. While fibrosis-4 index, aspartate aminotransferase to platelet ratio index, and LSM are widely used clinical tools, our radiomics models demonstrated superior AUCs. Overall, our findings suggest that machine learning can effectively predict LREs in patients with fibrosis and chronic hepatitis B, demonstrating comparable accuracy across algorithms and underscoring radiology's potential to enhance clinical decision-making. This approach enables identifying patients who require more frequent follow-ups and extended therapy.

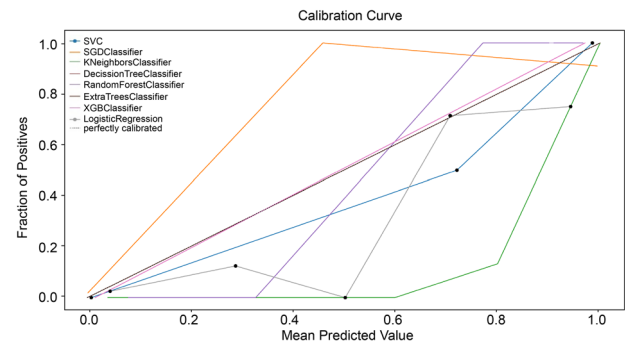


Fig. 5 Calibration curves of the radiomics models from different methods for the whole cohort. SGD, Stochastic gradient descent; SVC, Support vector machine classifier; XGB, Extreme gradient boosting

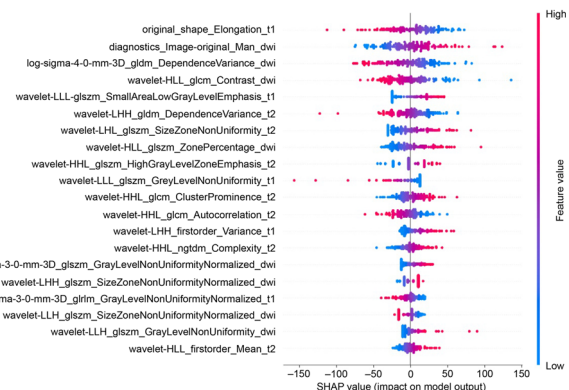


Fig. 6 SHAP values of the top 20 radiomics features as predictors of liver-related events. SHAP, SHapley Additive explanation

Liver function deteriorates at the cellular level due to damage or fibrosis, often associated with low-grade inflammation [28, 29]. Radiomics features capture subtle liver changes, offering a more precise representation of the complex physiopathological processes underlying LREs. Although MRI provides limited evidence of significant macroscopic liver alterations, fibrosis progression may lead to liver darkening, reduced blood flow, and decreased volume [30, 31]. Our models leverage these changes to predict LREs.

Fifty-eight radiomics features were extracted from liver MRI scans. Some were linked to liver shape (e.g., original-shape elongation), wavelets (e.g., Wavelet-HLL Gray Level Co-Occurrence Matrix Contrast), and texture (e.g., Gray-Level Non-Uniformity Normalized), all essential for predicting LREs. Notably, lower original-shape elongation values indicate rough, uneven liver edges. This aligns with prior research showing that fibrosis exacerbates liver fissures and shrinkage, impairing detoxification and compensatory function and ultimately increasing LRE risk [32]. Gray-level non-uniformity from GLSZM reflects grayscale heterogeneity in liver tissue, likely resulting from inflammation, fibrosis, nodules, and micronecrosis, all contributing to LRE

development [33]. Wavelet features are closely linked to cell morphology, pathophysiology, and proteomics. Notably, most of our study's final selected radiomics features were wavelet-based, aligning with findings from other radiomics research [34–36]. Overall, our MRI-based radiomics models exhibited strong predictive potential for improving outcomes in individuals with HBV-associated fibrosis. Our findings highlight the feasibility and clinical value of radiomics models in medical imaging analysis for predicting disease outcomes in chronic liver disease. We recommend a more aggressive monitoring and treatment strategy for high-risk patients identified on baseline MRI radiomics. This approach may involve increasing follow-up frequency, shortening intervals for high-risk patients to closely monitor disease progression for early diagnosis and screening of LREs. Extending the treatment cycle is another strategy, allowing longer treatment durations or dose adjustments within guideline recommendations to prevent LREs more effectively. Additionally, enhancing patient education for high-risk individuals can improve understanding of their condition and the importance of adherence, thereby boosting treatment compliance.

This study has limitations. First, its retrospective, single-center design may restrict the generalizability of our models. External validation, a larger sample size, and prospective studies are necessary to establish a more reliable predictive model. Second, while machine learning models can predict medical outcomes, data availability and accessibility must be carefully assessed, as they directly impact clinical applicability. This study's manual liver segmentation ensured accuracy but required substantial time and effort. In the future, greater emphasis should be placed on semi-automatic and automatic liver tissue segmentation methods. Third, the imaging-based model was not integrated with a clinical indicator model. This limitation may have hindered our understanding of the relationship between imaging findings and clinical outcomes, potentially reducing the model's overall effectiveness in predicting and monitoring patient outcomes. Future studies integrating imaging biomarker models with clinical indicators could enhance prognostic accuracy.

In conclusion, we developed a radiomics model using liver MRI, which may enhance risk prediction and management in patients with HBV-associated chronic fibrosis. This model offers valuable prognostic insights and supports clinical decision-making. Our model may help predict LRE risk in this patient population. Further research and validation are needed to confirm the clinical utility of this radiomics approach in managing HBV-associated chronic fibrosis.

Patient data cannot be publicly shared due to privacy concerns, but may be obtained from the corresponding

author upon reasonable request, subject to approval by the institutional review board of Zhuhai People's Hospital (xwg315@163.com).

Abbreviations

3D	Three-dimensional
AUC	Area under the receiver operating characteristic curve
DWI	Diffusion-weighted imaging
GLSZM	Gray Level Size Zone Matrix
HBV	Hepatitis B virus
LASSO	Least absolute shrinkage and selection operator
LRE	Liver-related event
LSM	Liver stiffness measurement
MRI	Magnetic resonance imaging

Supplementary information

The online version contains supplementary material available at <https://doi.org/10.1186/s41747-025-00602-0>.

Additional file 1: Fig. S1. Feature coefficient weight map. **Supplemental Fig. S2.** Box-and-whisker plots and waterfall plots of the radiomics score (Rad score) derived from the Least Absolute Shrinkage and Selection Operator (LASSO) feature for predicting liver-related events (LREs) in hepatitis B virus (HBV)-associated cirrhosis patients receiving oral antivirals. A, D: Entire primary cohort. B, E: Training cohort. C, F: Test cohort. The label '0' indicates patients without LRE, whereas the label '1' represents patients with LRE. **Supplemental Fig. S3.** Receiver operating characteristic curve analysis of Fibrosis 4 Score (FIB-4), aminotransferase-to-platelet ratio index (APRI), and liver stiffness measurement (LSM). **Supplemental Fig. S4.** Relative confusion matrices of the models in the training cohort (A) and test cohort (B). Model performances in the training cohort (C) and test cohort (D). **Supplemental Fig. S5.** Weights of radiomics signature importance.

Acknowledgements

The authors did not use any Large Language Models or other generative AI software for the preparation of the manuscript.

Author contributions

YKL, QNL, and YBW conducted the study, analyzed the data, and drafted the manuscript. YKL, HR, XFW, XJL, QY, and YL collected and verified the data. SRZ, WGX, XJL, and XFW developed and validated the methodology. YL and QSW supervised the study design and contributed to manuscript preparation. All authors reviewed and approved the final manuscript.

Funding

This study was supported by the National Natural Science Foundation of China (grant number 22207040), the Special Fund for Tumor Minimally Invasive Diagnosis and Treatment Translational Medicine Innovation Platform (no. 2021PY-01), and the Nurture Program of Zhuhai People's Hospital (no. 2021PY-02). The funder provided input on the study design. However, the funders did not have a role in the data collection, analysis, or preparation of the manuscript. The authors maintain full responsibility for the content and conclusions presented in this manuscript.

Data availability

Patient data cannot be publicly shared due to privacy concerns, but may be obtained from the corresponding author upon reasonable request, subject to approval by the institutional review board of Zhuhai People's Hospital (xwg315@163.com).

Declarations

Ethics approval and consent to participate

This study adhered to the Declaration of Helsinki and was approved by the Ethics Committee of Zhuhai People's Hospital (Approval Number 37 (2021)).

Consent for publication

Due to its retrospective design, the need for informed consent was waived. All patient records were anonymized and de-identified before analysis.

Competing interests

The authors declare that they have no competing interests.

Author details

¹Hepatobiliary and Pancreatic Tumor Diagnosis and Treatment Center, Yuebei People's Hospital, Shaoguan, China. ²Zhuhai Interventional Medical Center, Zhuhai People's Hospital (Zhuhai Clinical Medical College of Jinan University), Zhuhai, China. ³Department of Pain Management, Shaoguan Zhengtong Hospital, Shaoguan, China. ⁴Infection and Hepatology Department, Zhuhai Clinical Medical College of Jinan University (Zhuhai People's Hospital), Zhuhai, China. ⁵Department of Ultrasound Medicine, Zhanjiang Central People's Hospital, Zhanjiang, China. ⁶School of Medicine, Sun Yat-sen University, Shenzhen, China. ⁷Department of Radiology, Zhuhai People's Hospital (Zhuhai Clinical Medical College of Jinan University), Zhuhai, China.

Received: 17 September 2024 Accepted: 11 June 2025

Published online: 27 August 2025

References

- Chen S, Li J, Wang D, Fung H, Wong LY, Zhao L (2018) The hepatitis B epidemic in China should receive more attention. *Lancet* 391:1572. [https://doi.org/10.1016/S0140-6736\(18\)30499-9](https://doi.org/10.1016/S0140-6736(18)30499-9)
- Liu J, Fan D (2007) Hepatitis B in China. *Lancet* 369:1582–1583. [https://doi.org/10.1016/S0140-6736\(07\)60723-5](https://doi.org/10.1016/S0140-6736(07)60723-5)
- You H, Wang F, Li T et al (2023) Guidelines for the prevention and treatment of chronic hepatitis B, version 2022. *J Clin Transl Hepatol* 11:1425–1442
- European Association for the Study of the Liver (2018) EASL recommendations on treatment of hepatitis C 2018. *J Hepatol* 69:461–511. <https://doi.org/10.1016/j.jhep.2018.03.026>
- Dusheiko G, Agarwal K, Maini MK (2023) New approaches to chronic hepatitis B. *N Engl J Med* 388:55–69. <https://doi.org/10.1056/NEJMra2211764>
- Peng CY, Chien RN, Liaw YF (2012) Hepatitis B virus-related decompensated liver cirrhosis: benefits of antiviral therapy. *J Hepatol* 57:442–450. <https://doi.org/10.1016/j.jhep.2012.02.033>
- Ramos-Rincon JM, Pinargote-Celorio H, de Mendoza C et al (2022) Liver cancer and hepatic decompensation events in patients hospitalized with viral hepatitis in Spain. *Hepatol Int* 16:1161–1169. <https://doi.org/10.1007/s12072-022-10365-0>
- Boursier J, Hagström H, Ekstedt M et al (2022) Non-invasive tests accurately stratify patients with NAFLD based on their risk of liver-related events. *J Hepatol* 76:1013–1020. <https://doi.org/10.1016/j.jhep.2021.12.031>
- Pons M, Rodríguez-Tajes S, Esteban JI et al (2020) Non-invasive prediction of liver-related events in patients with HCV-associated compensated advanced chronic liver disease after oral antivirals. *J Hepatol* 72:472–480. <https://doi.org/10.1016/j.jhep.2019.10.005>
- Loomba R, Adams LA (2020) Advances in non-invasive assessment of hepatic fibrosis. *Gut* 69:1343–1352. <https://doi.org/10.1136/gutjnl-2018-317593>
- Belghiti J, Cauchy F, Paradis V, Vilgrain V (2014) Diagnosis and management of solid benign liver lesions. *Nat Rev Gastroenterol Hepatol* 11:737–749. <https://doi.org/10.1038/nrgastro.2014.151>
- Lambin P, Leijenaar RTH, Deist TM et al (2017) Radiomics: the bridge between medical imaging and personalized medicine. *Nat Rev Clin Oncol* 14:749–762. <https://doi.org/10.1038/nrclinonc.2017.141>
- Lambin P, Rios-Velazquez E, Leijenaar R et al (2012) Radiomics: extracting more information from medical images using advanced feature analysis. *Eur J Cancer* 48:441–446. <https://doi.org/10.1016/j.ejca.2011.11.036>
- Parmar C, Grossmann P, Bussink J, Lambin P, Aerts HJWL (2015) Machine learning methods for quantitative radiomic biomarkers. *Sci Rep* 5:13087. <https://doi.org/10.1038/srep13087>
- Zhang X, Wong GLH, Yip TCF et al (2022) Risk of liver-related events by age and diabetes duration in patients with diabetes and nonalcoholic fatty liver disease. *Hepatology* 76:1409–1422. <https://doi.org/10.1002/hep.32476>
- Elkrief L, Ganne-Carrié N, Manceau H et al (2023) Hepatocyte-derived biomarkers predict liver-related events at 2 years in Child-Pugh Class A alcohol-related cirrhosis. *J Hepatol* 79:910–923. <https://doi.org/10.1016/j.jhep.2023.05.025>
- Crispin-Ortuzar M, Woitek R, Reinius MAV et al (2023) Integrated radiogenomics models predict response to neoadjuvant chemotherapy in high grade serous ovarian cancer. *Nat Commun* 14:6756. <https://doi.org/10.1038/s41467-023-41820-7>
- Zhou J, Sun H, Wang Z et al (2023) Guidelines for the diagnosis and treatment of primary liver cancer, 2022 edn. *Liver Cancer* 12:405–444
- Fornacon-Wood I, Mistry H, Ackermann CJ et al (2020) Reliability and prognostic value of radiomic features are highly dependent on choice of feature extraction platform. *Eur Radiol* 30:6241–6250. <https://doi.org/10.1007/s00330-020-06957-9>
- Rodríguez-Pérez R, Bajorath J (2020) Interpretation of compound activity predictions from complex machine learning models using local approximations and Shapley values. *J Med Chem* 63:8761–8777. <https://doi.org/10.1021/acs.jmedchem.9b01101>
- Altmann A, Toloşi L, Sander O, Lengauer T (2010) Permutation importance: a corrected feature importance measure. *Bioinformatics* 26:1340–1347. <https://doi.org/10.1093/bioinformatics/btq134>
- Watson DS, Krutzinna J, Bruce IN et al (2019) Clinical applications of machine learning algorithms: beyond the black box. *BMJ* 364:l886. <https://doi.org/10.1136/bmj.l886>
- Boesch C (2018) Quantitative MR imaging is increasingly important in liver disease. *Radiology* 286:557–559. <https://doi.org/10.1148/radiol.2017172312>
- Boll DT, Merkle EM (2009) Diffuse liver disease: strategies for hepatic CT and MR imaging. *Radiographics* 29:1591–1614. <https://doi.org/10.1148/rg.296095513>
- van Herven JR, Marsman HA, Nederveen AJ et al (2010) Assessment of hepatic steatosis in patients undergoing liver resection: comparison of US, CT, T1-weighted dual-echo MR imaging, and point-resolved 1H MR spectroscopy. *Radiology* 256:159–168. <https://doi.org/10.1148/radiol.10091790>
- He L, Li H, Dudley JA et al (2019) Machine learning prediction of liver stiffness using clinical and T2-weighted MRI radiomic data. *AJR Am J Roentgenol* 213:592–601. <https://doi.org/10.2214/AJR.19.21082>
- Chen H, Zhang X, Wang X et al (2021) MRI-based radiomics signature for pretreatment prediction of pathological response to neoadjuvant chemotherapy in osteosarcoma: a multicenter study. *Eur Radiol* 31:7913–7924. <https://doi.org/10.1007/s00330-021-07748-6>
- Albillos A, Martín-Mateos R, Van Der Merwe S, Wiest R, Jalan R, Álvarez-Mon M (2022) Cirrhosis-associated immune dysfunction. *Nat Rev Gastroenterol Hepatol* 19:112–134. <https://doi.org/10.1038/s41575-021-00520-7>
- Trebicka J, Amoros A, Pitarch C et al (2019) Addressing profiles of systemic inflammation across the different clinical phenotypes of acutely decompensated cirrhosis. *Front Immunol* 10:476. <https://doi.org/10.3389/fimmu.2019.00476>
- Koda M, Murawaki Y, Kawasaki H, Ikawa S (1996) Portal blood velocity and portal blood flow in patients with chronic viral hepatitis: relation to histological liver fibrosis. *Hepatogastroenterology* 43:199–202
- Bak S, Kim JE, Bae K et al (2020) Quantification of liver extracellular volume using dual-energy CT: utility for prediction of liver-related events in cirrhosis. *Eur Radiol* 30:5317–5326. <https://doi.org/10.1007/s00330-020-06876-9>
- Yang Y, Fu S, Cao B et al (2021) Prediction of overt hepatic encephalopathy after transjugular intrahepatic portosystemic shunt treatment: a cohort study. *Hepatol Int* 15:730–740. <https://doi.org/10.1007/s12072-021-10188-5>
- Cannella R, Borhani AA, Tublin M, Behari J, Furlan A (2019) Diagnostic value of MR-based texture analysis for the assessment of hepatic fibrosis in patients with nonalcoholic fatty liver disease (NAFLD). *Abdom Radiol (NY)* 44:1816–1824. <https://doi.org/10.1007/s00261-019-01931-6>

34. Zhou Y, Zhou G, Zhang J, Xu C, Wang X, Xu P (2021) Radiomics signature on dynamic contrast-enhanced MR images: a potential imaging biomarker for prediction of microvascular invasion in mass-forming intrahepatic cholangiocarcinoma. *Eur Radiol* 31:6846–6855. <https://doi.org/10.1007/s00330-021-07793-1>
35. Ma X, Qian X, Wang Q et al (2023) Radiomics nomogram based on optimal VOI of multi-sequence MRI for predicting microvascular invasion in intrahepatic cholangiocarcinoma. *Radiol Med* 128:1296–1309. <https://doi.org/10.1007/s11547-023-01704-8>
36. Liang W, Xu L, Yang P et al (2018) Novel nomogram for preoperative prediction of early recurrence in intrahepatic cholangiocarcinoma. *Front Oncol* 8:360. <https://doi.org/10.3389/fonc.2018.00360>

Publisher's Note

Springer Nature remains neutral with regard to jurisdictional claims in published maps and institutional affiliations.